



## Article

# Ecological Security Assessment of “Grain-for-Green” Program Typical Areas in Northern China Based on Multi-Source Remote Sensing Data

Xingtao Liu <sup>1,2</sup>, Hang Li <sup>1</sup>, Shudong Wang <sup>1,3,\*</sup>, Kai Liu <sup>1,3</sup> , Long Li <sup>1,2</sup> and Dehui Li <sup>1,2</sup>

- <sup>1</sup> State Key Laboratory of Remote Sensing Science, Aerospace Information Research Institute, Chinese Academy of Sciences, Beijing 100194, China; liuxingtao21@mails.ucas.ac.cn (X.L.); lihang02@aircas.ac.cn (H.L.); liuk@aircas.ac.cn (K.L.); lilong22@mails.ucas.ac.cn (L.L.); lidehui22@mails.ucas.ac.cn (D.L.)
- <sup>2</sup> University of Chinese Academy of Sciences, Beijing 100049, China
- <sup>3</sup> Collaborative Innovation Center on Forecast and Evaluation of Meteorological Disasters (CIC-FEMD), Nanjing University of Information Science & Technology, Nanjing 210044, China
- \* Correspondence: wangsd@aircas.ac.cn; Tel.: +86-13121019866

**Abstract:** The Inner Mongolia segment of the Yellow River basin (IMYRB) is a typical area for ecological restoration in China. At the end of the 20th century, influenced by climate and human activities, such as mining, grazing, and farmland abandonment, the ecological security of the IMYRB was under more significant pressure. To alleviate the pressure on natural ecosystems and improve the fragile ecological situation, China implemented the “Grain-for-Green” (GFG) project in 1999. However, the evolutionary characteristics of the ecological security of the IMYRB in the first two decades of the 21st century are still lacking. Quantitative and long-term ecological security information of “Grain-for-Green” is needed. Based on this, this study used the “Pressure (P)-State (S)-Response (R)” method and proposed an ecological security assessment and early warning system based on multi-source remote sensing data. The evaluation results indicated a significant improvement in ecological security in the IMYRB from 2000 to 2020. Compared to 2000, the ecological security of the IMYRB had improved significantly in 2020, with an increase of 11.02% (ES > 0.65) and a decrease of 8.89% (ES < 0.35). For the early warning aspect of ecological security, there was a 26.31% growth in non-warning areas, with a 5% decrease in warning areas. Based on the analysis of ecologically critical factors, we proposed the implications for future ecological management as follows. (1) In ecologically fragile areas such as the IMYRB, continued implementation of the GFG was necessary. (2) Vegetation restoration should be scientific and tailored adaptive. (3) The protection of arable land also showed necessity. (4) The grazing management skills should be upgraded. Our study demonstrated that the ecological benefits derived from the “GFG” project are not immediate but cumulative and persistent. The continuous implementation of “GFG” will likely alleviate the pressure exerted by human activities on the natural environment.



**Citation:** Liu, X.; Li, H.; Wang, S.; Liu, K.; Li, L.; Li, D. Ecological Security Assessment of “Grain-for-Green” Program Typical Areas in Northern China Based on Multi-Source Remote Sensing Data. *Remote Sens.* **2023**, *15*, 5732. <https://doi.org/10.3390/rs15245732>

Academic Editor: Aolin Jia

Received: 14 October 2023

Revised: 7 December 2023

Accepted: 12 December 2023

Published: 15 December 2023



**Copyright:** © 2023 by the authors. Licensee MDPI, Basel, Switzerland. This article is an open access article distributed under the terms and conditions of the Creative Commons Attribution (CC BY) license (<https://creativecommons.org/licenses/by/4.0/>).

**Keywords:** ecological security assessment; “Grain-for-Green”; P-S-R; early warning

## 1. Introduction

In the late 20th century, influenced by farmland expansion, unsustainable grazing, and mining, the Inner Mongolia segment of the Yellow River basin (IMYRB) suffered land desertification [1], salinization [2], and biodiversity decline [3]. At the same time, global climate change has led to frequent regional extreme climate disasters [4]. In the 1990s, the IMYRB, as a typical ecologically fragile region, destroyed and degraded its ecological barriers, which were further aggravated by a combination of natural and anthropogenic disturbances [5,6], which posed a severe threat to regional ecological security [7].

In order to curb the deteriorating trend of ecological security and effectively engage in ecological conservation, China has undertaken various ecological governance projects

since the 21st century [8]. The “Grain-for-Green” project aims to make the steep farmland that caused high soil erosion and low yields out of cultivation [9,10]. Some studies suggest that the project effectively mitigated soil erosion [11,12], bolstered regional carbon sequestration [13–15], and significantly enhanced water retention capacity [16–18] and vegetation coverage [19]. However, at the early stage of “GFG”, the survival rate of trees was low due to the inadequacy of relevant regulations and forest management systems [20,21]. In addition, due to accelerated urbanization, many rural workforces moved to cities, leaving trees unattended [22,23]. Therefore, obtaining quantitative and precise information on the evolution of ecological security after implementing the GFG is imperative.

The Pressure–State–Response (P-S-R) model was widely applied in ecological environment safety evaluation assessment [24,25]. The P-S-R comprehensively considers the interaction between humans and ecosystems, which can be tailored to specific area conditions [26]. In P-S-R, “P” indicators refer to pressures on ecosystems, both natural and artificial. “S” reflects the state of the ecosystem, including vitality, resilience, and function [27,28]. The “R” dimension consists of indicators related to human activities, such as measures and policies [29,30].

Based on multi-source remote sensing data, the P-S-R model was built, which makes ecological security conducting high-efficiency [31–33]. However, the existing P-S-R does not reflect the “Grain-for-Green” impact on ecological security [34] due to the following reasons: (1) In the IMYRB, the ecological security situation is complex due to the many factors, such as the “GFG”, grazing, mineral exploitation, the growth of urbanization [35], undulating terrain, and uneven precipitation [36]. Most existing assessment systems had not adequately considered these factors. (2) Due to the lack of information on the spatial and temporal distribution of “GFG”, the relationship between “GFG” and ecosystem security cannot be effectively analyzed [37,38].

This study used multi-source remote sensing data to assess the ecological security in the IMYRB. Grazing and mining areas were included in the pressure dimension. We utilized ecosystem elasticity, vitality, and ecosystem service functions to characterize ecological security status. Furthermore, it is worth noting that we included “GFG” information in the response dimension. We established an integrated ecological security remote sensing evaluation and early warning system based on the Pressure–State–Response (P-S-R) framework, coupling human society, economic development, and natural ecosystems. This system assessed the ecological security changes in the IMYRB after “Grain-for-Green”, providing valuable data references for ecological management.

## 2. Study Area and Data

### 2.1. Study Area

The Inner Mongolia section of the Yellow River Basin (IMYRB) is located in the upper reaches of the Yellow River Basin in the western part of the Inner Mongolia Autonomous Region (38°26′~42°50′N, 106°59′~110°10′E). The altitude lies between 816 and 2393 m. The IMYRB is located in a semi-arid and arid region (Figure 1a) with an average annual precipitation of 297.25 mm [39]. The land cover types are diverse (Figure 1b). The dust storms during the spring are the main reason for wind erosion. And the heavy summer rainfall can be the primary factor leading to water erosion [40]. The IMYRB comprises a variety of functional zones, including the significant sand-producing tributary known as Ten Kongdui (ten major tributaries of the Yellow River, located in Ordos City, with an average annual sand loss of about 27 million tonnes) [41], the West Ordos National Nature Reserve, and the Hetao Irrigation Area (Figure 1c). It also encompasses the Hohhot–Baotou–Ordos urban cluster, which bolsters regional economic development. However, at the end of the 20th century, rapid urban development, mining, and land desertification had put pressure on ecosystems, resulting in heightened ecological vulnerability and a growing prominence of ecological issues. Therefore, to harmonize economic development with ecological conservation, China initiated the “Grain-for-Green (GFG)” project in 1999. After

1999, a significant amount of sloping farmland in the IMYRB had been converted to forest and grassland [9,10] (Figure 1d).

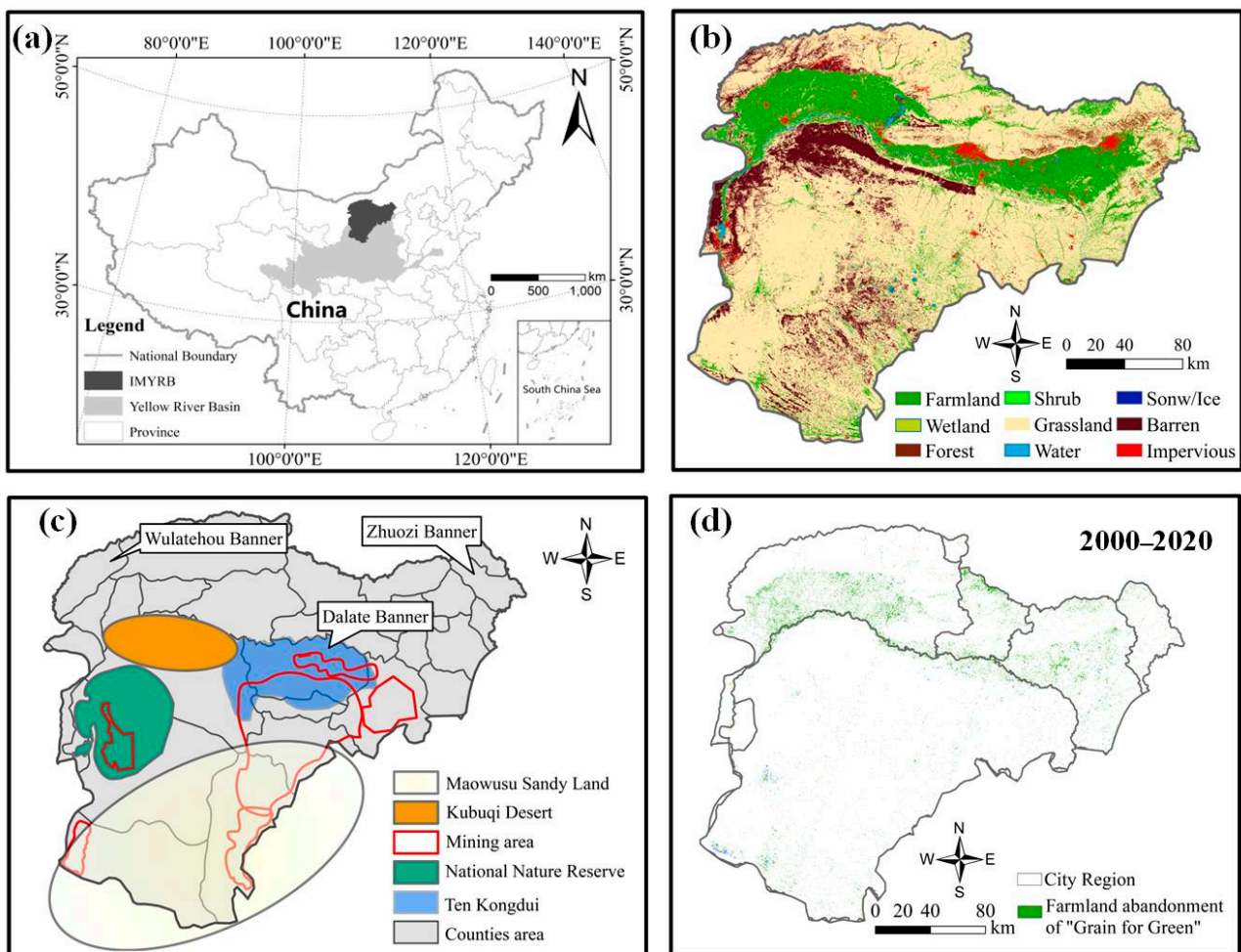


**Figure 1.** Spatial distribution, land cover types, function areas, and farmland abandonment information in the IMYRB. (a) is the geographical location of the IMYRB. (b) shows the land cover types. (c) presents the crucial ecological function areas, including MuUs Sandland, Kubuqi Desert, the mining area, the National Nature Reserve, and Ten Kongdui. (d) is the farmland abandonment area of the IMYRB.

## 2.2. Data and Pre-Processing

We used diverse remote sensing data, including land cover, climate, vegetation indices, nighttime light, and terrain (Table 1). The WGS84 UTM 48N projection was adopted to maintain the spatial consistency of each index.

Specifically, the China Land Cover Dataset (CLCD, 30 m), released by Professors Jie Yang and Xin Huang from Wuhan University on Zenodo [42], with a high spatial resolution of 30 m, was often used as input data for land use dynamics detection (Figure 1c).

The terrain slope data were derived from SRTM DEM (30 m) elevation data jointly measured by NASA (National Aeronautics and Space Administration) and NIMA (National Imagery and Mapping Agency). The slope data were used as one of the inputs for calculating topographic indices and ecology services [43].

The TerraClimate precipitation dataset was generated using climate-aided interpolation techniques, which combined high spatial resolution climate data from WorldClim with multiple low-resolution datasets, such as CRU and JRA55 [44]. The MOD13Q1 NDVI (16-day, 250 m), MOD16A2 (8-day, 500 m), and MOD17A2H GPP (8-day, 500 m) were sourced from the National Aeronautics and Space Administration (NASA) [45–47], which

were used to analyze the vegetation recovery after farmland abandonment. MOD16A2 (8-day, 500 m) was a global terrestrial evapotranspiration product that can be used to study regional water energy balances [48]. Based on this, NDVI, GPP, and ET datasets were pre-processed using the MODIS Reprojection Tool (MRT), which included tasks such as mosaicking, projection, format conversion, and resampling.

**Table 1.** Multi-source remote sensing data information.

No.	Dataset	Product Type	Data Type	Resolution	The Date of Collection	Data Source
1	MODIS	MOD13Q1	NDVI	250 m/16 d	2000–2020	<a href="https://ladsweb.modaps.eosdis.nasa.gov/search/">https://ladsweb.modaps.eosdis.nasa.gov/search/</a>
2		MOD17A2H	GPP	500 m/8 d	2000, 2020	
3		MOD16A2	Evaporation	500 m/8 d	2000, 2010, 2020	
4	CLCD	-	Land cover	30 m/year	2000–2020	<a href="https://doi.org/10.5194/essd-13-3907-2021">https://doi.org/10.5194/essd-13-3907-2021</a>
5	GlobeLand30	-	Land cover	30 m/year	2000, 2010, 2020	
6	SRTM	SRTMGL1_003	Digital elevation data	30 m	2019	<a href="https://doi.org/10.1029/2005RG000183">https://doi.org/10.1029/2005RG000183</a> .
7	TerraClimate	-	Precipitation	4 km/month	2000, 2010, 2020	<a href="https://www.climatologylab.org/terraclimate.html">https://www.climatologylab.org/terraclimate.html</a>
8	Nighttime Data	DMSP/OLS NPP/VIIRS	Nighttime Data	1 km resampled	2000, 2010, 2020	<a href="https://www.ngdc.noaa.gov/eog/download.html">https://www.ngdc.noaa.gov/eog/download.html</a>
9						
10	HWSD	-	Harmonized World Soil Database	-	2000, 2010, 2020	<a href="https://www.fao.org/">https://www.fao.org/</a>
11	Miner and protected area data	Vectorization data	-	-	2000–2020	<a href="https://doi.org/10.1016/j.jhydrol.2020.125759">https://doi.org/10.1016/j.jhydrol.2020.125759</a> <a href="https://doi.org/10.3390/su8090889">https://doi.org/10.3390/su8090889</a>

Nightlight data can represent the human activity intensity effectively. In this study, DMSP/OLS and NPP/VIIRS Nighttime Data were obtained from the National Oceanic and Atmospheric Administration (NOAA) National Centers for Environmental Information. We conducted saturation, consistency, and continuity calibration on the nighttime light data and resampled them to achieve a consistent spatial resolution of 1 km [49,50].

Statistical data were used to analyze the state of ecological security of the IMYRB since 2000. The mining areas and protected zone data were obtained through literature research [51,52]. GDP, year-end population, year-end livestock herds, afforested area, and cultivated area are from the Statistics Bureau of Inner Mongolia (<http://tj.nmg.gov.cn/>) (accessed on 10 May 2023). Owing to data availability, the number of livestock was obtained only for 2000 and 2010. The World Soil Attributes Database (HWSD), as reliable soil data, was also used for ecology assessment [53].

### 3. Methods

#### 3.1. Remote Sensing Ecological Security Assessment Indicator System

The Pressure–State–Response (P–S–R) model was introduced by the Organization for Economic Cooperation and Development (OECD) and the United Nations Environment Programme (UNEP) in the 1980s. Due to the combination of natural and anthropogenic impacts on ecosystems, the P–S–R method shows the merits of ecological and environmental security assessment [32,54]. For assessing ecological security on the IMYRB, the Ecological Security Index (ESI) was established [33,34,55].

##### 3.1.1. P–S–R Ecological Security Index Selection

This P–S–R assessment framework comprises three dimensions (Pressure, State, and Response). Given each indicator’s impact on ecological security, these indicators were categorized into positive (+) and negative (–). The content and method of P–S–R were developed and enriched by combining natural and human impacts in Table 2.

**Table 2.** Ecological safety assessment system (3 km).

Goal	Dimension (Weight)	Indicator (Weight)	Equation	Description (±)	
Pressure (P) (0.249)		Precipitation Index (PI) (0.228)	$PI_i = \frac{\sum_{j=1}^n PI_{ij} \cdot S_0}{PI_{i,max} \cdot S_i}$	$P_{ij}$ is the annual precipitation of Year j in assessment unit i, $S_0$ and $S_i$ are the areas of the image and assessment unit i, respectively, and $PI_{i,max}$ is the maximum annual precipitation in assessment unit i. (+)	
		Terrain index (TI) (0.174)	$TI_i = \frac{\sum_{j=1}^n TI_{ij} \cdot S_0}{TI_{max,i} \cdot S_i} \cdot f_i$ $f_i = \sigma_i / u_i$	$TI_{ij}$ is the slope of year j in assessment unit i, and $TI_{max,i}$ is the maximum TI in unit i. $f_i$ , $\sigma_i$ and $u_i$ are the coefficient of variation, standard deviation and mean of the slope, respectively. (-)	
		Mining Area Index (MAI) (0.284)	$MI_i = \frac{\sum_{j=1}^n MI_{ij} \cdot S_0}{MI_{max,i} \cdot S_i}$	$MI_{ij}$ is the MI of Year j in unit i, and $MI_{max,i}$ is the maximum MI in unit i (-)	
		Disturbance Index (DI) (0.598)	Grazing intensity Index (GII) (0.258)	$GII_i = \frac{\sum_{j=1}^n GII_{ij} \cdot S_0}{GII_{max,i} \cdot S_i}$	$GII_{ij}$ is the GII of Year j in unit i, and $GII_{max,i}$ is the maximum MI in unit i (-)
		Population Density Index (PII) (0.458)	$PII_i = h_i \cdot \frac{\sum_{j=1}^n UI_{ij} \cdot S_0}{UI_{max,i} \cdot S_i}$ $h_i = (L_i - L_{min}) - (L_{max} - L_{min})$	UI is the urbanization index which refers to the urban areas. $UI_{ij}$ is the UI of Year j in unit i, and $UI_{max,i}$ is the maximum MI in unit i. $L_i$ is the light data index. $L_{min}$ and $L_{max}$ are the minimum and maximum values of light luminance in the study area, respectively (-)	
Ecological security Index		Ecosystem Resilience Index (ERI) (0.156)	$ERI_i = \frac{\sum_{j=1}^n ERI_{ij} \cdot S_0}{ERI_{max,i} \cdot S_i}$	$ERI_{ij}$ is the elasticity coefficient for land cover type j in assessment unit i. $ERI_{max,i}$ is the maximum ERI in unit i (+)	
		Ecosystem Vitality Index (EVI) (0.222)	$EVI_i = \frac{\sum_{j=1}^n NDVI_{ij} \cdot S_0}{NDVI_{i,max} \cdot S_i}$	$NDVI_{ij}$ is the elasticity coefficient of year j in assessment unit i. $NDVI_{i,max}$ is the maximum NDVI in unit i (+)	
		Landscape Fragmentation Index (LFI) (0.173)	$LFI_i = \frac{\sum_{j=1}^n PD_{ij} \cdot S_0}{PD_{max,i} \cdot S_i}$ $PD_i = N / TA$	$PD_{ij}$ is the patch density for land cover type j in assessment unit i. $PD_{max,i}$ is the maximum PD in unit i. N is the of patches in landscape i, and TA is the total area of landscape i. (-)	
		Carbon storage and sequestration (0.2)	$C_i = \frac{\sum_{j=1}^n C_{ij} \cdot S_0}{C_{max,i} \cdot S_i}$ $C_{(total)} = C_{(above)} + C_{(below)} + C_{(soil)} + C_{(dead)}$	$C_{ij}$ is the carbon for land cover type j in assessment unit i. $C_{max,i}$ is the maximum C in unit i. $C_{above}$ , $C_{below}$ , $C_{soil}$ and $C_{dead}$ are the above-ground fraction carbon stock, below-ground fraction carbon stock, soil carbon stock and dead organic carbon stock, respectively. (+)	
Statement (S) (0.594)		Ecosystem Services Index (ESI) (0.449)	Water Yield Model (0.2)	$WR_i = \frac{\sum_{j=1}^n WR_{ij} \cdot S_0}{WR_{max,i} \cdot S_i}$ $Y = (1 - \frac{AET}{P}) * P$ $WR = Y - Runoff$ $Runoff = P * C$	$WR_{ij}$ is the water retention for land cover type j in assessment unit i. $WR_{max,i}$ is the maximum water retention in unit i. $Y_x$ is the water yield (mm); $AET$ is the actual annual average evapotranspiration of grid cell (mm); $P$ is the annual average precipitation of grid cell (mm). $WR$ is the water retention (mm); $Runoff$ is the amount of surface runoff (mm); and $C$ is the surface runoff coefficient, which expresses the ability of precipitation to be converted into runoff. (+)
			Sediment Delivery Ratio (0.6)	$SDR_i = \frac{\sum_{j=1}^n SDR_{ij} \cdot S_0}{SDR_{max,i} \cdot S_i}$ $SDR = RKLS - USLE + SEDR$	$SDR_{ij}$ is the sediment delivery ratio for land cover type j in assessment unit i. $SDR_{max,i}$ is the maximum sediment delivery ratio in unit i. $SDR$ , $RKLS$ , $USLE$ and $SEDR$ denote the amount of soil retention, potential erosion, actual erosion, and retention, respectively. (+)

**Table 2.** Ecological safety assessment system (3 km).

Goal	Dimension (Weight)	Indicator (Weight)	Equation	Description ( $\pm$ )
Ecological security Index	Response (R) (0.157)	Protected Area Index (PAI) (0.5)	$PAI_i = \frac{\sum_{j=1}^n PAI_{ij} \cdot S_0}{PAI_{\max,i} \cdot S_i}$	$PAI_{ij}$ is the protected district area for land cover type $j$ in assessment unit $i$ . $PAI_{\max,i}$ is the maximum protected district area in unit $i$ . (+)
		Farmland Abandonment and Recultivation Index (FARI) (0.5)	$FARI_i = (k_1 \cdot \frac{\sum_{j=1}^n FA_{ij}}{S_i} - k_2 \cdot \frac{\sum_{j=1}^n FR_{ij}}{S_i}) \cdot S_0$	$FA_{ij}$ and $FR_{ij}$ Are the areas of farmland abandonment and recultivation for land cover type $j$ in assessment unit $i$ . $k_1$ and $k_2$ are 0.65 and 0.35, respectively. (+)

### 1. Ecological system pressure (P) index selection

Ecological system pressure (P) describes the extent to which an ecosystem faces disturbances. Specifically, terrain is variable at spatial scales [54], although the spatial extent of the IMYRB is small. The IMYRB is located in an arid and semi-arid region, where spatial heterogeneity of precipitation can have an impact on ecological status [56]. The IMYRB is a major coal-producing region in China. Mining can put more pressure on the ecological environment [57]. The IMYRB is also a typical agricultural and pastoral zone in northern China, and agriculture and animal husbandry are the main modes of production [58]. In addition, the rapid development of urbanization in the IMYRB since the 21st century has led to the over-occupation of land resources and ecological damage, which has put greater pressure on the ecological environment [59]. To conduct quantitative studies of urbanization, the night light data were used [60]. In this study, three indices were chosen to reflect the pressure on ecosystems under the influence of both natural and human disturbances: Precipitation Indices (PI), Topographic Indices (TI), and the Disturbance Index (DI). Grazing intensity (GI), Mining area index (MI), and the Population Density Index (PDI) were selected to show the disturbance of human activities on the ecosystem of the IMYRB, namely the Disturbance Index (DI).

### 2. Ecological System Status (S) Index Selection

Ecosystem status (S) refers to the health and ecological environmental quality of an ecosystem. Four indicators were selected to reflect the state of the ecosystem in the IMYRB. Land use conditions reflect the interaction between human activities and natural conditions [61], while NDVI can capture vegetation information, representing richness and activity [59]. The Landscape Fragmentation Index (LFI), an indicator of human interference, characterizes the degree of fragmentation where the landscape is divided. Mining, grazing, and urban expansion had increased land use fragmentation in the IMYRB [62].

Additionally, the shortage of water resources is a major constraint on the coordinated economic and ecological development of the IMYRB [63]. Wind and water erosion are the main causes of soil erosion [64]. Changes in ecosystem services had a direct impact on ecosystem security [65]. In the IMYRB, ecosystem service is an effective indicator of ecological security [66]. Integrated Valuation of Ecosystem Services and Tradeoffs (InVEST), as an open-source software model, was often used to map ecological services, including carbon, seasonal water yield sediment retention modules, and so on [54,67]. Integrated valuation for ecosystem services and tradeoffs (InVEST) is being applied to decision-making involving more sustainable choices to assess ecosystem services [68,69]. In this study, carbon sequestration, soil erosion, and water resource conservation were calculated using InVEST as indicators of the Ecological Service Index (ESI). Therefore, the Ecological system status (S) index includes the Ecological Resilience Index (ERI), Ecological Vitality Index (EVI), Landscape Fragmentation Index (LFI), and Ecosystem Service Index (ESI), respectively.

### 3. Ecological System Response (R) Index Selection

Ecosystem response (R) refers to the ability of an ecosystem to mitigate the effects of a disturbance through its anti-disturbance mechanisms or anthropogenic measures. It

is worth mentioning that China's "GFG" project aims to convert farmland into forest or grassland, resulting in high ecological significance against ecological vulnerability [70]. Implementing "GFG" has proven effective and beneficial in reducing soil erosion, land desertification, and other related issues, thereby enhancing the quality of ecological security [20]. At the same time, in order to protect the redline for arable land, there have been efforts to recultivation [71]. Moreover, the proportion of protected ecological functional areas represents the extent of ecological protection and the potential for enhancing ecological security [72]. In conclusion, we have incorporated the Farmland Abandonment and Recultivation Index (FARI) and the Protected Area Index (PAI) into the ecological security response indicators for the IMYRB.

### 3.1.2. Establishment of Ecological Security Index System Based on P-S-R

The creation of a grid of reasonable dimensions is necessary. Currently, in order to effectively reflect the spatial heterogeneity of each indicator, most ecological security studies tend to use a grid ranging from 1 km to 5 km [73–77]. As the data we used were of large spatial extent, ranging from 30 m to 4 km, the 3 km × 3 km grid is suitable to make the indicators spatially consistent.

To assess ecosystem services, we employed the InVEST assessment model. The InVEST Carbon Storage and Sequestration model uses maps of land use along with stocks in carbon pools to estimate the amount of carbon currently stored in a landscape or the amount of carbon sequestered over time [78]. In this study, we used the CLCD landcover data and the carbon pools data, which were acquired by <https://naturalcapitalproject.stanford.edu/> (accessed on 15 December 2022). The sediment retention service provided by vegetation is of great interest to water managers and land managers [79]. DEM elevation data, TerraClimate annual precipitation, and soil erodibility data were used to acquire the sediment delivery ratio. We combined this with precipitation data, CLCD land use products, plant-available soil moisture data (from the Chinese Academy of Sciences Nanjing Institute of Soil Science's 1:100,000 soil dataset), and HWSO to evaluate regional water yield.

Apart from this, We used CLCD land use data from 2000 to 2020 to extract the active farmland area per year by reclassification. On this basis, we carried out change detection. In our view, for a pixel, if the previous year was arable land and the next year was non-arable land, it was considered to be abandoned farmland. If the farmland was abandoned in the previous year but active in the current year, it was considered recultivated farmland.

### 3.1.3. Determination of Indicator Weights

Indicator weights refer to the relative importance of a specific indicator in relation to the evaluation object or evaluation target within an evaluation system. The Analytic Hierarchy Process (AHP) is a method used to decompose elements related to evaluation objectives into different levels and perform qualitative or quantitative analysis to determine the weights of each indicator [80,81]. In this study, the four-level indicator system was developed by analyzing relevant studies and consulting the Inner Mongolia Autonomous Region Ecological Environment Related Committee experts. Among them, the first level of indicators is ecological safety, and P, S, and R are the second level indicators. The third level indicators were the specific factors of P, S, and R. The last level indicators were the indexes for calculating disturbance index and ecosystem services. Four questionnaires were administered to each of the five academic experts and four governmental experts (Table 2).

### 3.1.4. Standardization and Calculation of Ecological Security Indicators

Data standardization was used due to the different indicators [82]. We categorized the indicators into two groups: positive and negative. For positive indicators, a larger value indicated better ecological security. In contrast, for negative indicators, the smaller the value, the better the ecological security. The formulas are as follows:

Positive:

$$Z_{mn} = \frac{X_{mn} - \min(X_m)}{\max(X_m) - \min(X_m)} \quad (1)$$

Negative:

$$Z_{mn} = 1 - \frac{X_{mn} - \min(X_m)}{\max(X_m) - \min(X_m)} \tag{2}$$

In the formula,  $Z_{mn}$  is the standardized value of the indicator  $m$  in the year  $n$ ;  $X_{mn}$  is the original value of the indicator  $m$  in the year  $n$ ;  $\max(X_m)$  and  $\min(X_m)$  are the maximum and minimum values of the indicator  $m$  in the year  $n$ , respectively.  $m$  represents the number of indicators.

In this study, we utilized the AHP to assign weights to various levels of indicators (refer to Section 3.1.1). Based on this, we calculated the Ecological Security Index by combining the standardized values of indicators with their respective weights. The calculation formula is as follows:

$$ESI_n = \sum_{i=1}^m Z_{mn} \times W_{mn} \tag{3}$$

In the formula,  $Z_{mn}$  represents the standardized value of the indicator  $m$  in the year  $n$ ,  $W_{mn}$  is the weight of the indicator  $m$  in the year  $n$ .  $m$  represents the number of indicators.

### 3.2. Ecological Security Assessment System and Early Warning System Establishment

At present, there is no unified classification standard for ecological security. Related studies [58,73,83] have categorized ESI into different levels. This study used spatial analysis by Arcgis 10.6 and divided ecological security into five intervals (Table 3). Early warning systems for ecosystems are commonly used to determine the trend and rate of ecosystem change [84] and provide a basis for determining the sequence of ecological restoration [85]. In this study, the critical values for different stages of the warning system were determined by calculating  $\Delta ESI$  (changes of ESI) between adjacent time intervals and grading ESI (Table 4).

**Table 3.** Ecological safety index (ESI) classification in the IMYRB.

ESI Level	Low	Mid-Low	Medium	Mid-High	High
Ecology Security Index Statement	ESI ≤ 0.35 Unsafe	0.35 < ESI < 0.45 Less safe	0.45 < ESI < 0.55 Critical Safe	0.55 < ESI < 0.65 Relatively Safe	ESI ≥ 0.65 Safe
Ecosystem Structure	Lack	Serious damage	Destruction	More structured	Integrity
Ecosystem Function	Serious damage	High difficulty	Appearance of destruction	Robust	Sound

**Table 4.** Ecological security warning (ESW) system in the IMYRB.

	ESI Level	ESI Statement	ΔESI	Analysis	Level of ESW
Ecological Security Warning (ESW)	ESI ≥ 0.55	Safe	ΔESI > 0	Non-warning	I
			ΔESI < 0	Non-warning, Degradation trend	II
			ΔESI > 0	Early warning, Improvement trend	III
	0.35 < ESI < 0.55	Critical Safe	0 < ΔESI < 0.1	Early warning, Slow degradation trend	IV
			ΔESI < 0	Early warning, Rapid degradation trend	V
	ESI ≤ 0.35	Unsafe	ΔESI > 0	Warning, Improvement trend	VI
			ΔESI < 0	Warning, Degradation trend	VII

## 4. Results

### 4.1. Ecological Safety Assessment in the IMYRB

We established a 3 km × 3 km grid network as the assessment unit. Using the Analytic Hierarchy Process (AHP), we assigned weights to different indicators in the P-S-R evaluation system (Table 2). Based on this, we created an ecological security map of the IMYRB and conducted statistics on the proportions of ecological security at different levels (Figure 2).

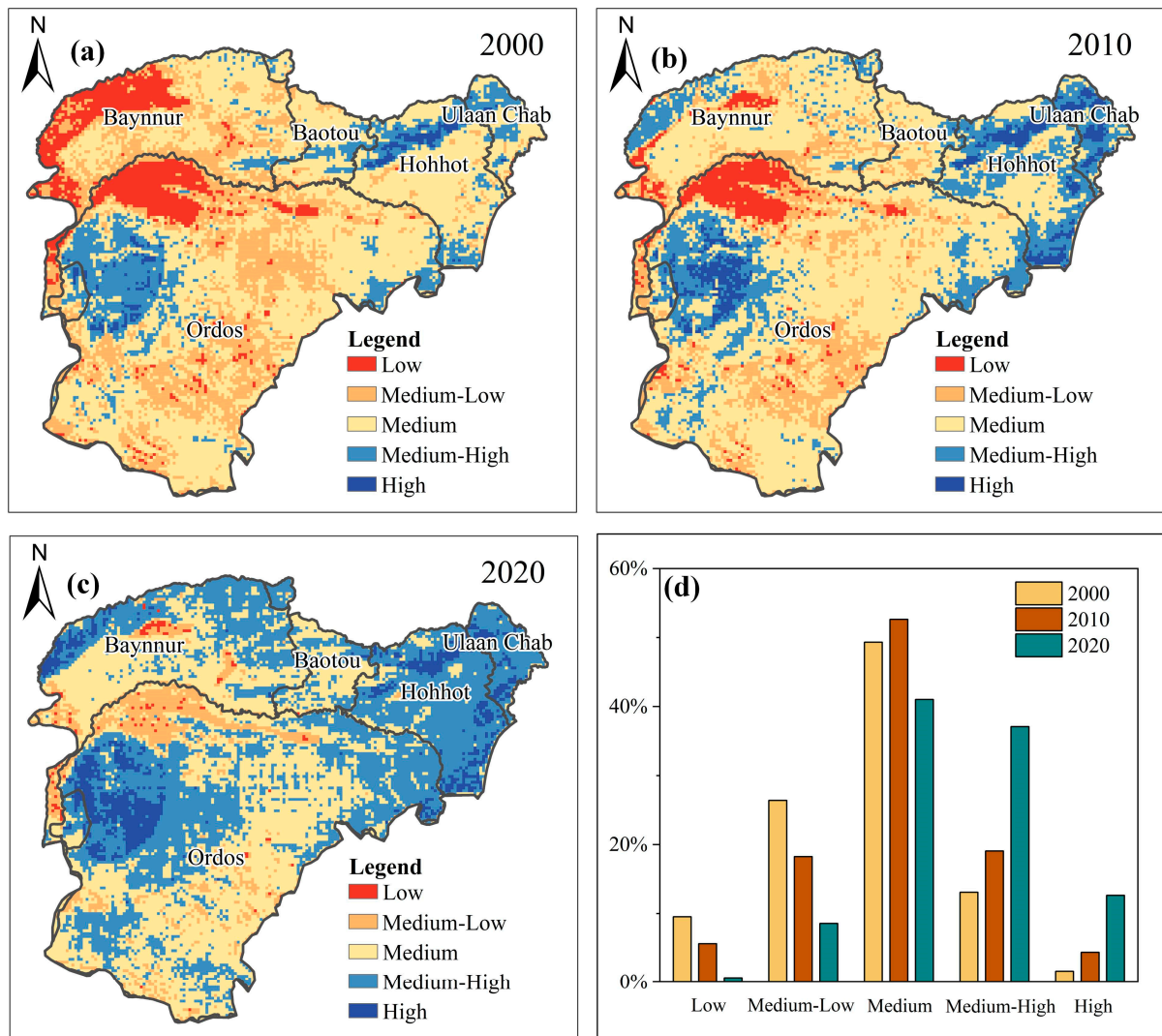


**Figure 2.** Ecological security and its percentage of security levels in the IMYRB from 2000 to 2020. (a–c) are ecological security assessment results in 2000, 2010, and 2020, respectively. (d) is the percentage of different ecological security levels.

Ecological security zones (medium-high and high) in the IMYRB are primarily located in the western part of Etooke Banner, the Western Ordos National Nature Reserve within the territory of Wuhai City, Hohhot City, and Zhuozhi County in Ulanqab City (Figure 1c). The ecological security (ES) in the reserve had consistently been high (greater than 0.55), and over the past two decades, the high-value ES zone has radiated outward from this reserve, increasing the total area by 51,849 km<sup>2</sup>. Compared to 2000, the ecological security of the IMYRB had improved significantly in 2020, with an increase of 11.02% (ES > 0.65) (Figure 2). Ecological critical zones (mid-value and mid-low value) are mainly distributed in the eastern hilly and gully areas of Ordos City, the central Mu Us Sandland, and the Hetao Plain (Figure 1c). Among these, from 2000 to 2020, the mid-value zone showed an overall trend of increase followed by a decrease in 2010 (from 49.3% to 52.65% and then to 41.06%). The area proportion of mid-low value zones notably decreased (from 26.41% to 8.58%) (Figure 2d). Ecological low-value proportion experienced a decrease of 8.89%, from 14,166 km<sup>2</sup> to 963 km<sup>2</sup>. Overall, from 2000 to 2020, with the continuous commencement of “GFG” and afforestation initiatives, the ecological security situation in the IMYRB steadily improved.

#### 4.2. Dynamic Analysis of Ecological Security Early Warning

According to the ecological security warning (ESW) system, we categorized the ESW into seven levels (Table 4). We mapped the ESW in 2000–2020 in the IMYRB by using a  $3\text{ km} \times 3\text{ km}$  grid (Figure 3). From 2000 to 2020, the unsafe regions in the IMYRB notably decreased, with the warning-degradation areas and warning-improvement areas reduced by 3.47% and 1.53%, respectively. The critical safety zones decreased by over 20%, while the safe areas significantly increased (>25%) (Figure 3).

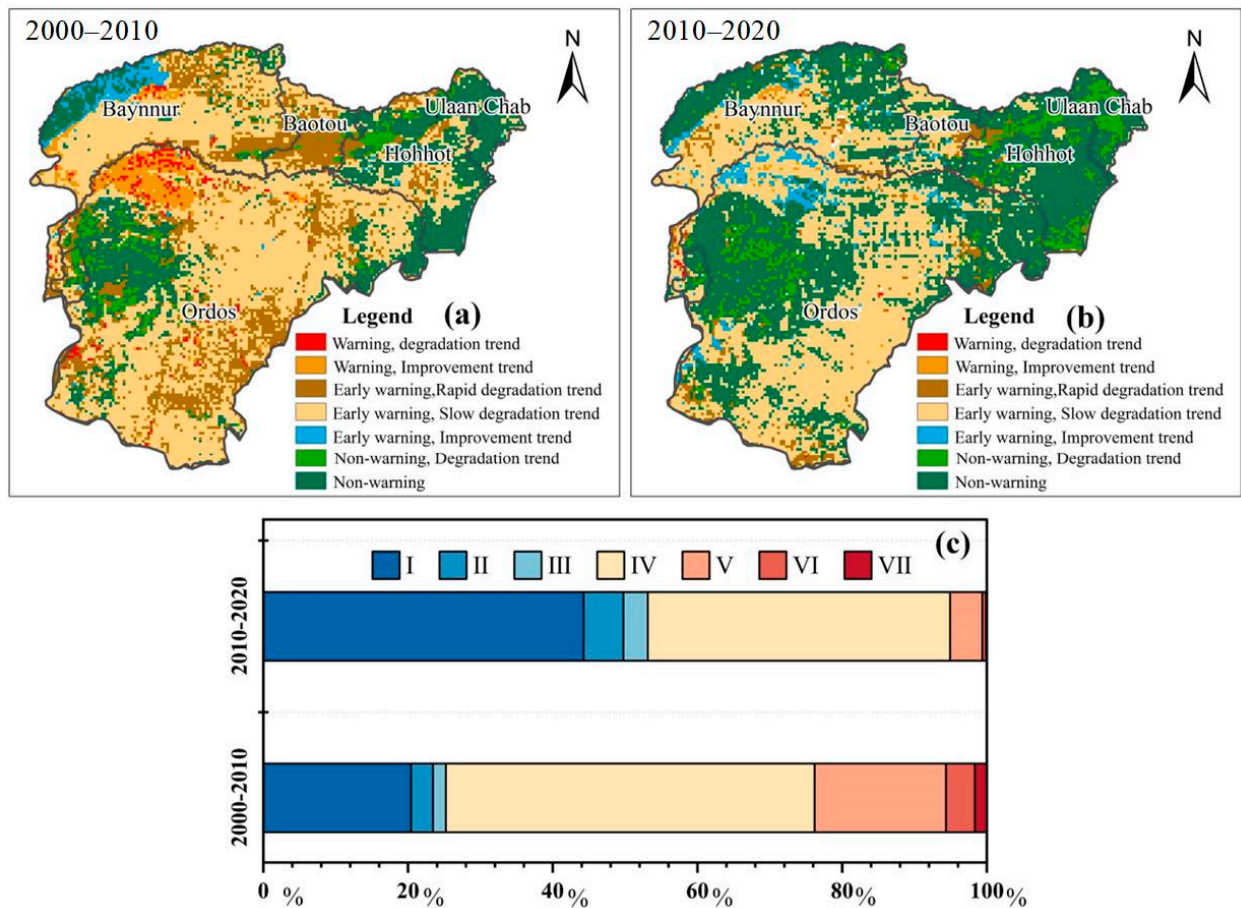


**Figure 3.** Ecological security early warning and percentage of in the IMYRB from 2000 to 2020. (a,b) are ecological security early warnings in 2000–2010 and 2010–2020, respectively. (c) is the proportions of the different ecological security warning areas in the IMYRB.

Based on the above analysis, the ecological warning status in the IMYRB showed an overall positive trend. The warning conditions gradually improved from the surrounding areas towards the center. In the western part of Ordos City, the ecological security zone radiates outward from the ecological protection area (Figure 1c). In the northwest desert areas (Figure 1c), there had been a significant transition from ecological warning to ecological critical safety. The ecological security of Baynnur had improved. Ulaan Chab and Baotou can also see improvements in their ecological security conditions and were essentially in a non-warning state. These results suggested a positive ecological trend in the IMYRB, with areas gradually transitioning to more secure ecological states, especially in the central and northern regions.

## 5. Discussion

### 5.1. Ecological Security Assessment System Rationality and Data Reliability

In this study, we selected ecological security assessment indicators and created a  $3\text{ km} \times 3\text{ km}$  grid to quantitatively assess the ecological security spatiotemporal changes.

The impact of climate and human disturbance on ecological security cannot be ignored. This study considered the impact of natural and anthropogenic factors on ecological security. Grazing intensity, “Grain-for-Green” areas, protected areas, and mining areas were included in the evaluation system using spatial analyses. In addition, we used InVEST to capture ecosystem services scientifically. Night light data were used to quantify urban development. To acquire the farmland abandonment dataset, we used CLCD land use data from 2000 to 2020 to extract the cultivated land area per year by reclassification. Based on reliable datasets, we established an ecological security indicator system tailored for the IMYRB in conjunction with the “GFG” policy.

### 5.2. Possible Mechanism of ES Improvement and Policy Implications

The results of the integrated policy measures and ecological vulnerability assessment indicate that the ecological security of the IMYRB is affected by a variety of factors. The main reasons for the improvement in ecological security include water use and management policies, environmental protection of these changes, and restoration projects [86].

#### 5.2.1. The Implementation of the GFG Can Be Effective in Enhancing Ecological Security

Socio-economic, e.g., GDP, population, and grazing development, had put greater anthropogenic pressure on the ecological security of the IMYRB (Figure 4a–c). In the face of increasing pressure on ecosystems, sustained implementation of ecological conservation policies was necessary. On the other hand, in the first two decades of the 21st century, ecological security has increased significantly (0–20%). This was attributed to China’s emphasis on ecological protection in the process of economic development. It can be seen that from 2000 to 2020, there was a huge increase in NDVI and GPP. NDVI and GPP in typical areas of “GFG”, such as the Zhungeer banner, showed high growth rates of 61.51% and 31.55%, respectively, which implied an increase in ecosystem vitality (Figure 4e,f). Therefore, the effectiveness of the “GFG” implementation can be recognized.

Furthermore, we combined the CLCD (30 m) land use data with SRTM DEM (30 m) data to extract the farmland whose slopes were over 25°. The extraction results showed that there are still 3.234 km<sup>2</sup> of sloping farmland with slopes greater than 25° in the IMYRB. Thus, for the areas where farmland was still cultivated in an unjustified way, it was necessary to conduct “GFG” further in the future.

#### 5.2.2. Scientific Vegetation Restoration Is an Effective Way to Improve Ecological Security

To quantify the impact of the “GFG” on regional ecological security further, we took Ordos City as an example. We collected and analyzed data related to farmland abandonment, reforestation, and human activity pressures.

The improvement in ecological security due to “GFG” was a cumulative process and had a lag in ecological security enhancement. We believe that this may be related to the maturity of afforested trees and their adaptation to the local environment. Young trees planted initially can quickly increase vegetation coverage in the region in the short term. However, their primary productivity was limited, which means their capacity to improve the regional ecological environment is also limited [87]. In some cases, the short-term sharp increase in water consumption by regional vegetation can temporarily increase the water resource pressure on the ecosystem [88], leading to a temporary decline in ecosystem security. It is only when these young trees gradually mature and adapt to the local natural and geographical environment that their contribution to ecosystem security becomes evident.

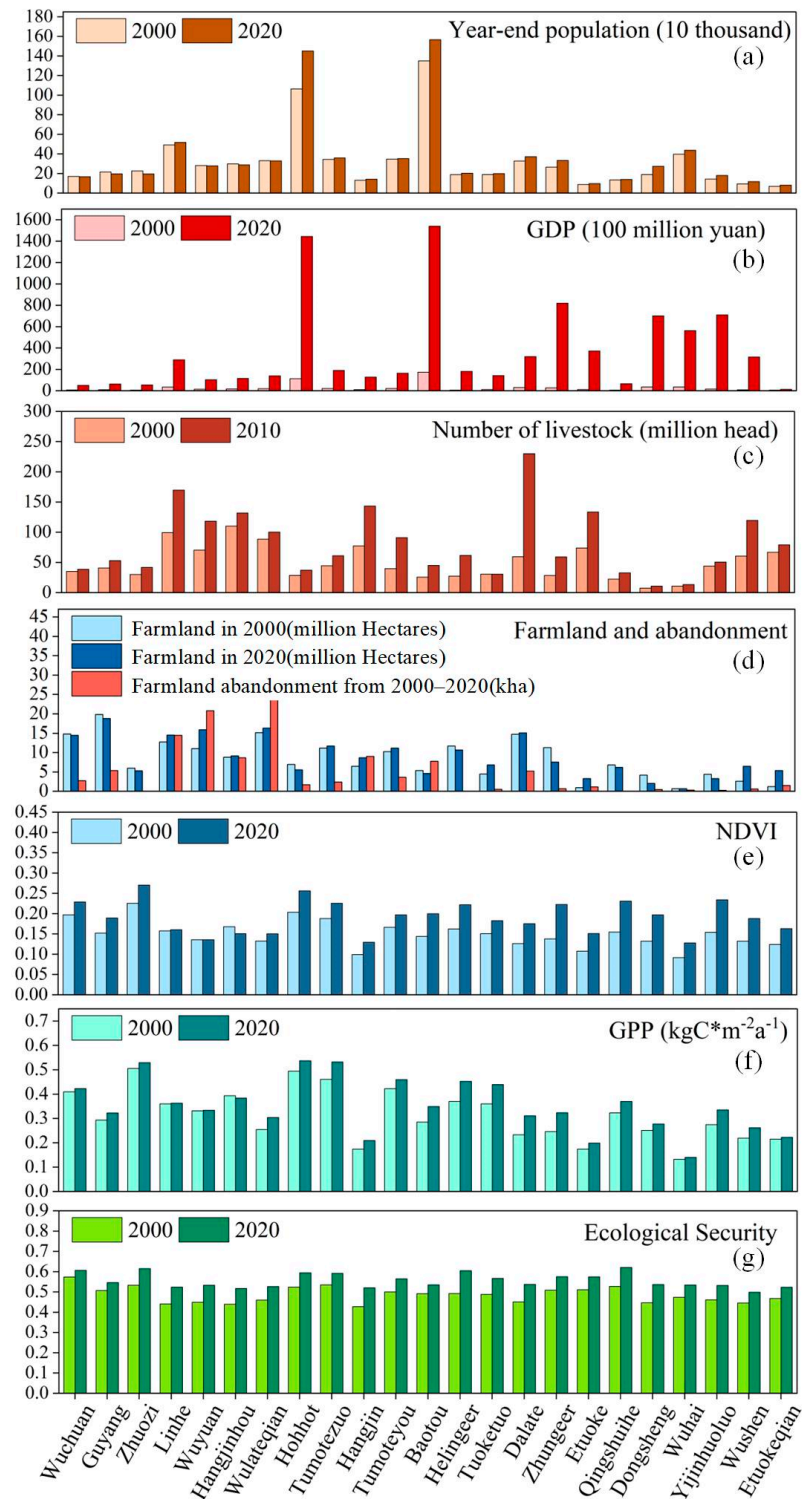


**Figure 4.** Key Factors of Districts and Counties in the IMYRB from 2000 to 2020. (a–g) are Year-end Population, GDP, Number of Livestock, Farmland and abandonment, NDVI, GPP, and Ecological security in the IMYRB in 2000 and 2020.

### 5.2.3. The “Red Line” of Arable Land Should Be Kept in “Grain-for-Green”

Excessive farmland abandonment posed a challenge to agricultural security and food security. In Erdos, compared to 2000, the amount of abandoned farmland was significantly reduced by 10% (Figure 5). Protection of farmland, which was suitable for cultivation, has

shown more importance in recent years. Therefore, protecting the red line of arable land showed a high degree of necessity.

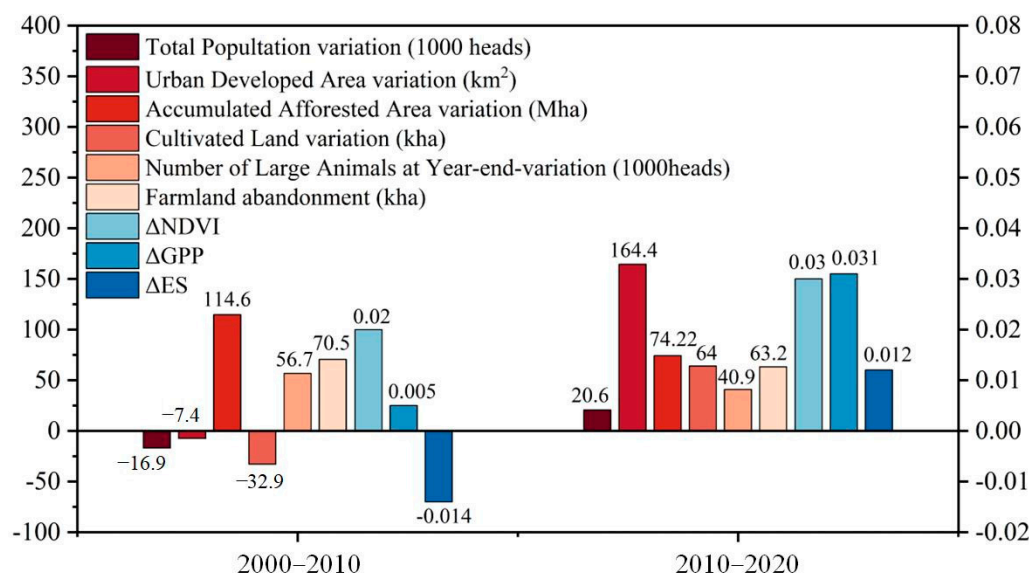


**Figure 5.** Key Factors of Districts and Counties in the IMYRB from 2000 to 2020. The Total Population variation, Urban Developed area, Accumulated Afforested Area variation, Cultivated Land variation, Number of Large Animals and Farmland abandonment should refer to the left  $y$ -axis. And  $\Delta$ NDVI,  $\Delta$ GPP, and  $\Delta$ ES should refer to the right  $y$ -axis.

#### 5.2.4. Upgrading Grazing Management Skills Is Essential for Grassland Ecological Security

Livestock populations had generally experienced a trend of increase in 2000–2010 (Figure 4c) followed by a decrease of about 10% (Figure 5).

From the results described above, it is apparent that ecological restoration policies can effectively change the ecological vulnerability pattern. Ecological restoration has achieved remarkable results in the IMYRB. The land use type of the IMYRB was dominated by grasslands. It was undeniable that appropriate grazing can maintain or even increase carbon stocks and protect grasslands by reducing plant diseases. However, when the grazing intensity exceeds the threshold, the ecosystem can be degraded [89]. In recent years, China has introduced several grazing management policies in Inner Mongolia, but grassland management still lacks scientific and technical guidance. Therefore, it is necessary to improve grassland management skills to meet the needs of grazing and protect the ecological stability of grasslands.

#### 5.3. Limitations and Perspectives

In future work, we need to improve the following aspects further: (1) Spatial applicability of the assessment indicator system: This study effectively screened the indicator system applicable to arid and semi-arid fallow forest areas in northern China. However, due to the heterogeneity between northern and southern China, the applicability of this indicator system should be carried out. The ecological security assessment of the “GFG” program in southern China or in a large region needs to be considered. In addition, this study does not include indicators for characterizing vegetation water stress, which is necessary for arid and semi-arid areas to be included in future studies. (2) Applicability of the grid: A 3 km  $\times$  3 km grid was selected as the evaluation unit in this study, which can better show the ecological security status of the IMYRB. If the whole Yellow River Basin or a larger scale is evaluated, the evaluation unit needs to be re-established according to the basin condition.

## 6. Conclusions

The IMYRB is a typical area in northern China that is experiencing the implementation of the “GFG” program. In this study, we used the P-S-R ecological evaluation method, coupled with multi-source remote sensing data, to construct an ecological security assessment system and early warning system applicable to the area of returning farmland to forest.

The research indicated that from 2000 to 2020, there had been a continuous improvement in the ecological security of the IMYRB. The ecological warning areas had decreased significantly, going from over 20% to below 10%. This marked a significant improvement in the quality of the ecological environment. However, from 2000 to 2010, there was not a widespread and substantial improvement in ecological security, with the ecological security zone increasing by only 8% and the unsafe zone decreasing by 12%. By 2020, there had been a noticeable improvement in ecological security both in terms of regional scale and the extent of change. The ecological security zone had increased by 35%, with over 50% of the region covered by ecological security zones. This suggested that the impact of the “GFG” program on ecological security was not immediate. The impact of the “GFG” program on ecological security was characterized by its persistence and cumulative nature.

This research highlighted the significant impact of the “GFG” program on ecological security in the IMYRB. To maintain and enhance the current ecological security status in this region, it is necessary to continue the implementation of the program. It is important to consider the local climatic and hydrological conditions during the process of “GFG”, adopting an approach that combines natural recovery with artificial restoration. Apart from this, regular assessments should also be conducted to ensure the orderly and effective operation of the program.

**Author Contributions:** X.L. was responsible for the experiment design, data curation, visualization, and manuscript preparation. H.L. contributed to the conceptualization and review of the manuscript. S.W. contributed to the conceptualization, review, and funding acquisition. K.L. contributed to the review. L.L. contributed to partial data curation and manuscript review. D.L. contributed to partial data curation and manuscript editing. All authors have read and agreed to the published version of the manuscript.

**Funding:** This research was supported by the Key Program of the Institute (E2Z211020F), the National Natural Science Foundation of China (NO. 42141007), and the Science and Technology Planning Project of Hohhot (2022-soical-key-4-1-1).

**Data Availability Statement:** Data are contained within the article.

**Acknowledgments:** The authors would like to thank the anonymous reviewers and editors.

**Conflicts of Interest:** The authors declare no conflict of interest.

## References

1. Smil, V. *China's Environmental Crisis: An Enquiry into the Limits of National Development*; Routledge: London, UK, 2016.
2. Li, S.; Yang, S.; Liu, X.; Liu, Y.; Shi, M. NDVI-based analysis on the influence of climate change and human activities on vegetation restoration in the Shaanxi-Gansu-Ningxia Region, Central China. *Remote Sens.* **2015**, *7*, 11163–11182. [[CrossRef](#)]
3. Li, L.; Zhan, W.; Hu, L.; Chakraborty, T.; Wang, Z.; Fu, P.; Wang, D.; Liao, W.; Huang, F.; Fu, H. Divergent urbanization-induced impacts on global surface urban heat island trends since 1980s. *Remote Sens. Environ.* **2023**, *295*, 113650. [[CrossRef](#)]
4. Kucharczyk, M.; Hugenholtz, C.H. Remote sensing of natural hazard-related disasters with small drones: Global trends, biases, and research opportunities. *Remote Sens. Environ.* **2021**, *264*, 112577. [[CrossRef](#)]
5. Zhao, Y.; Zeng, Y.; Zheng, Z.; Dong, W.; Zhao, D.; Wu, B.; Zhao, Q. Forest species diversity mapping using airborne LiDAR and hyperspectral data in a subtropical forest in China. *Remote Sens. Environ.* **2018**, *213*, 104–114. [[CrossRef](#)]
6. Ma, C.; Qian, Y.; Li, K.; Dou, X.; Shen, H.; Tang, H.; Qiu, S.; Zhang, L.; Jia, Y.; Ou-Yang, G. Temperature and Emissivity Retrieval from Hyperspectral Thermal Infrared Data Using Dictionary-Based Sparse Representation for Emissivity. *IEEE Trans. Geosci. Remote Sens.* **2023**, *61*, 1–16. [[CrossRef](#)]
7. Liu, D.; Chang, Q. Ecological security research progress in China. *Acta Ecol. Sin.* **2015**, *35*, 111–121. [[CrossRef](#)]
8. Lü, Y.; Fu, B.; Feng, X.; Zeng, Y.; Liu, Y.; Chang, R.; Sun, G.; Wu, B. A policy-driven large scale ecological restoration: Quantifying ecosystem services changes in the Loess Plateau of China. *PLoS ONE* **2012**, *7*, e31782. [[CrossRef](#)]

9. Li, Y. Grain-for-Green program is a great concrete action towards the ecological civilization in China: Summary of a decade program implementation. *For. Constr.* **2009**, *27*, 3–13.
10. Bennett, M.T. China's sloping land conversion program: Institutional innovation or business as usual? *Ecol. Econ.* **2008**, *65*, 699–711. [[CrossRef](#)]
11. Lei, D.; Shangguan, Z.P.; Rui, L. Effects of the grain-for-green program on soil erosion in China. *Int. J. Sediment Res.* **2012**, *27*, 120–127.
12. Zhang, X.Y.; Liu, K.; Li, X.K.; Wang, S.D.; Wang, J.N. Vulnerability assessment and its driving forces in terms of NDVI and GPP over the Loess Plateau, China. *Phys. Chem. Earth* **2022**, *125*, 103106. [[CrossRef](#)]
13. Deng, L.; Liu, G.B.; Shangguan, Z.P. Land-use conversion and changing soil carbon stocks in China's 'Grain-for-Green' Program: A synthesis. *Glob. Chang. Biol.* **2014**, *20*, 3544–3556. [[CrossRef](#)] [[PubMed](#)]
14. Li, H.; Yang, B.H.; Meng, Y.; Liu, K.; Wang, S.D.; Wang, D.C.; Zhang, H.Y.; Huang, Y.L.; Liu, X.T.; Li, D.H.; et al. Relationship between carbon pool changes and environmental changes in arid and semi-arid steppe—A two decades study in Inner Mongolia, China. *Sci. Total Environ.* **2023**, *893*, 164930. [[CrossRef](#)] [[PubMed](#)]
15. Bo, Y.; Li, X.K.; Liu, K.; Wang, S.D.; Zhang, H.Y.; Gao, X.J.; Zhang, X.Y. Three Decades of Gross Primary Production (GPP) in China: Variations, Trends, Attributions, and Prediction Inferred from Multiple Datasets and Time Series Modeling. *Remote Sens.* **2022**, *14*, 2564. [[CrossRef](#)]
16. Liu, K.; Li, X.K.; Wang, S.D.; Zhou, G.S. Past and future adverse response of terrestrial water storages to increased vegetation growth in drylands. *NPJ Clim. Atmos.* **2023**, *6*, 113. [[CrossRef](#)]
17. Liu, K.; Li, X.K.; Wang, S.D.; Zhang, X.Y. Unrevealing past and future vegetation restoration on the Loess Plateau and its impact on terrestrial water storage. *J. Hydrol.* **2023**, *617*, 129021. [[CrossRef](#)]
18. Li, D.H.; Liu, K.; Wang, S.D.; Wu, T.X.; Li, H.; Bo, Y.; Zhang, H.Y.; Huang, Y.L.; Li, X.K. Four decades of hydrological response to vegetation dynamics and anthropogenic factors in the Three-North Region of China and Mongolia. *Sci. Total Environ.* **2023**, *857*, 159546. [[CrossRef](#)] [[PubMed](#)]
19. Delang, C.O.; Yuan, Z. *China's Grain-for-Green Program*; Springer: Berlin/Heidelberg, Germany, 2016.
20. Li, G.; Sun, S.; Han, J.; Yan, J.; Liu, W.; Wei, Y.; Lu, N.; Sun, Y. Impacts of Chinese Grain-for-Green program and climate change on vegetation in the Loess Plateau during 1982–2015. *Sci. Total Environ.* **2019**, *660*, 177–187. [[CrossRef](#)]
21. Wu, X.; Wang, S.; Fu, B.; Feng, X.; Chen, Y. Socio-ecological changes on the Loess Plateau of China after Grain to Green Program. *Sci. Total Environ.* **2019**, *678*, 565–573. [[CrossRef](#)]
22. Delang, C.O. The second phase of the Grain-for-Green program: Adapting the largest reforestation program in the world to the new conditions in rural China. *Environ. Manag.* **2019**, *64*, 303–312. [[CrossRef](#)]
23. Wang, B.; Gao, P.; Niu, X.; Sun, J. Policy-driven China's Grain to Green Program: Implications for ecosystem services. *Ecosyst. Serv.* **2017**, *27*, 38–47. [[CrossRef](#)]
24. Wu, X.; Liu, S.; Sun, Y.; An, Y.; Dong, S.; Liu, G. Ecological security evaluation based on entropy matter-element model: A case study of Kunming city, southwest China. *Ecol. Indic.* **2019**, *102*, 469–478. [[CrossRef](#)]
25. Ma, L.; Bo, J.; Li, X.; Fang, F.; Cheng, W. Identifying key landscape pattern indices influencing the ecological security of inland river basin: The middle and lower reaches of Shule River Basin as an example. *Sci. Total Environ.* **2019**, *674*, 424–438. [[CrossRef](#)] [[PubMed](#)]
26. Chen, Y.; Wang, J. Ecological security early-warning in central Yunnan Province, China, based on the gray model. *Ecol. Indic.* **2020**, *111*, 106000. [[CrossRef](#)]
27. Fan, Y.; Fang, C. Evolution process and obstacle factors of ecological security in western China, a case study of Qinghai province. *Ecol. Indic.* **2020**, *117*, 106659. [[CrossRef](#)]
28. Yang, Y.; Song, G.; Lu, S. Assessment of land ecosystem health with Monte Carlo simulation: A case study in Qiqihaer, China. *J. Cleaner Prod.* **2020**, *250*, 119522. [[CrossRef](#)]
29. Zhang, Y.; Fan, J.; Wang, S. Assessment of ecological carrying capacity and ecological security in China's typical eco-engineering areas. *Sustainability* **2020**, *12*, 3923. [[CrossRef](#)]
30. Zhang, Y.; Zhang, L.; Yu, K.; Zou, Y. Analysis of the Characteristics of Ecological Security Zoning and Its Dynamic Change Pattern: A Case Study of the Weibei Area. *Sustainability* **2020**, *12*, 7222. [[CrossRef](#)]
31. Du, P.; Xia, J.; Du, Q.; Luo, Y.; Tan, K. Evaluation of the spatio-temporal pattern of urban ecological security using remote sensing and GIS. *Int. J. Remote Sens.* **2013**, *34*, 848–863. [[CrossRef](#)]
32. Lu, T.; Li, C.; Zhou, W.; Liu, Y. Fuzzy Assessment of Ecological Security on the Qinghai–Tibet Plateau Based on Pressure–State–Response Framework. *Remote Sens.* **2023**, *15*, 1293. [[CrossRef](#)]
33. Wen, J.; Hou, K.; Li, H.; Zhang, Y.; He, D.; Mei, R. Study on the spatial-temporal differences and evolution of ecological security in the typical area of the Loess Plateau. *Environ. Sci. Pollut. Res.* **2021**, *28*, 23521–23533. [[CrossRef](#)]
34. Lu, Y.; Wang, X.; Xie, Y.; Li, K.; Xu, Y. Integrating future land use scenarios to evaluate the spatio-temporal dynamics of landscape ecological security. *Sustainability* **2016**, *8*, 1242. [[CrossRef](#)]
35. Zhou, T.; Shen, W.; Qiu, X.; Chang, H.; Yang, H.; Yang, W. Impact evaluation of a payments for ecosystem services program on vegetation quantity and quality restoration in Inner Mongolia. *J. Environ. Manag.* **2022**, *303*, 114113. [[CrossRef](#)]
36. Zhang, H.; Zhang, J.; Lv, Z.; Yao, L.; Zhang, N.; Zhang, Q. Spatio-Temporal Assessment of Landscape Ecological Risk and Associated Drivers: A Case Study of the Yellow River Basin in Inner Mongolia. *Land* **2023**, *12*, 1114. [[CrossRef](#)]

37. Gao, Y.; Zhang, C.; He, Q.; Liu, Y. Urban ecological security simulation and prediction using an improved cellular automata (CA) approach—A case study for the city of Wuhan in China. *Int. J. Environ. Res. Public Health* **2017**, *14*, 643. [\[CrossRef\]](#)
38. Yu, H.; Yang, J.; Qiu, M.; Liu, Z. Spatiotemporal changes and obstacle factors of Forest ecological security in China: A provincial-level analysis. *Forests* **2021**, *12*, 1526. [\[CrossRef\]](#)
39. Ye, Z.; Miao, P.; Li, N.; Wang, Y.; Meng, F.; Zhang, R.; Yin, S. Dynamic Relationship between Agricultural Water Use and the Agricultural Economy in the Inner Mongolia Section of the Yellow River Basin. *Sustainability* **2023**, *15*, 12979. [\[CrossRef\]](#)
40. Wang, Y.; Wu, B.; Zhong, D.; Wang, Y. Calculation method for sediment load in flood and non-flood seasons in the Inner Mongolia reach of the Yellow River. *Geogr. Sci.* **2016**, *26*, 707–721. [\[CrossRef\]](#)
41. Yang, H.; Shi, C. Sediment grain-size characteristics and its sources of ten wind-water coupled erosion tributaries (the Ten Kongduis) in the Upper Yellow River. *Water* **2019**, *11*, 115. [\[CrossRef\]](#)
42. Yang, J.; Huang, X. The 30 m annual land cover dataset and its dynamics in China from 1990 to 2019. *Earth* **2021**, *13*, 3907–3925. [\[CrossRef\]](#)
43. Rabus, B.; Eineder, M.; Roth, A.; Bamler, R. The shuttle radar topography mission—A new class of digital elevation models acquired by spaceborne radar. *ISPRS J. Photogramm. Remote Sens.* **2003**, *57*, 241–262. [\[CrossRef\]](#)
44. Abatzoglou, J.T.; Dobrowski, S.Z.; Parks, S.A.; Hegewisch, K.C. TerraClimate, a high-resolution global dataset of monthly climate and climatic water balance from 1958–2015. *Sci. Data* **2018**, *5*, 170191. [\[CrossRef\]](#)
45. Pringle, M.; Denham, R.; Devadas, R. Identification of cropping activity in central and southern Queensland, Australia, with the aid of MODIS MOD13Q1 imagery. *Int. J. Appl. Earth Obs. Geoinf.* **2012**, *19*, 276–285. [\[CrossRef\]](#)
46. Gebremichael, M.; Barros, A.P. Evaluation of MODIS gross primary productivity (GPP) in tropical monsoon regions. *Remote Sens. Environ.* **2006**, *100*, 150–166. [\[CrossRef\]](#)
47. Running, S.W.; Thornton, P.E.; Nemani, R.; Glassy, J.M. Global terrestrial gross and net primary productivity from the earth observing system. In *Methods in Ecosystem Science*; Springer: New York, NY, USA, 2000; pp. 44–57.
48. Mu, Q.; Zhao, M.; Running, S.W. MODIS global terrestrial evapotranspiration (ET) product (NASA MOD16A2/A3). *Algorithm Theor. Basis Doc. Collect.* **2013**, *5*, 600.
49. Liu, Z.; He, C.; Zhang, Q.; Huang, Q.; Yang, Y. Extracting the dynamics of urban expansion in China using DMSP-OLS nighttime light data from 1992 to 2008. *Landscape Urban Plann.* **2012**, *106*, 62–72. [\[CrossRef\]](#)
50. Elvidge, C.D.; Ziskin, D.; Baugh, K.E.; Tuttle, B.T.; Ghosh, T.; Pack, D.W.; Erwin, E.H.; Zhizhin, M. A fifteen year record of global natural gas flaring derived from satellite data. *Engineering* **2009**, *2*, 595–622. [\[CrossRef\]](#)
51. Wang, W.; Liu, R.T.; Gan, F.P.; Zhou, P.; Zhang, X.W.; Ding, L. Monitoring and evaluating restoration vegetation status in mine region using remote sensing data: Case study in Inner Mongolia, China. *Remote Sens.* **2021**, *13*, 1350. [\[CrossRef\]](#)
52. Chen, G.Q.; Wang, M.J.; Liu, Z.J.; Chi, W.F. The biogeophysical effects of revegetation around mining areas: A case study of Dongsheng mining areas in Inner Mongolia. *Sustainability* **2017**, *9*, 628. [\[CrossRef\]](#)
53. Nachtergaele, F.; van Velthuisen, H.; Verelst, L.; Wiberg, D.; Henry, M.; Chiozza, F.; Yigini, Y. *Harmonized World Soil Database Version 2.0*; Food and Agriculture Organization of the United Nations: Rome, Italy, 2023.
54. Li, G.; Jiang, C.; Zhang, Y.; Jiang, G. Whether land greening in different geomorphic units are beneficial to water yield in the Yellow River Basin? *Ecol. Indic.* **2021**, *120*, 106926. [\[CrossRef\]](#)
55. Zhang, Y.; Zang, P.; Guo, H.; Yang, G. Wetlands ecological security assessment in lower reaches of Taoerhe river connected with Nenjiang river using modified P-S-R model. *Hydrol Res.* **2023**, *6*, 156–165. [\[CrossRef\]](#)
56. Jiang, W.; Yuan, L.; Wang, W.; Cao, R.; Zhang, Y.; Shen, W. Spatio-temporal analysis of vegetation variation in the Yellow River Basin. *Ecol. Indic.* **2015**, *51*, 117–126. [\[CrossRef\]](#)
57. Li, T.T.; Zhang, Q.; Wang, G.; Singh, V.P.; Zhao, J.Q.; Sun, S.; Wang, D.Z.; Liu, T.X.; Duan, L.M. Ecological degradation in the Inner Mongolia reach of the Yellow River Basin, China: Spatiotemporal patterns and driving factors. *Ecol. Indic.* **2023**, *154*, 110498. [\[CrossRef\]](#)
58. Zhang, X.; Liu, K.; Wang, S.; Wu, T.; Li, X.; Wang, J.; Wang, D.; Zhu, H.; Tan, C.; Ji, Y. Spatiotemporal evolution of ecological vulnerability in the Yellow River Basin under ecological restoration initiatives. *Ecol. Indic.* **2022**, *135*, 108586. [\[CrossRef\]](#)
59. Zhang, Z.; Liu, Y. Spatial Expansion and Correlation of Urban Agglomeration in the Yellow River Basin Based on Multi-Source Nighttime Light Data. *Sustainability* **2022**, *14*, 9359. [\[CrossRef\]](#)
60. Sang, S.; Wu, T.; Wang, S.; Yang, Y.; Liu, Y.; Li, M.; Zhao, Y. Ecological Safety Assessment and Analysis of Regional Spatiotemporal Differences Based on Earth Observation Satellite Data in Support of SDGs: The Case of the Huaihe River Basin. *Remote Sens.* **2021**, *13*, 3942. [\[CrossRef\]](#)
61. Zheng, Y.; Wang, S.; Cao, Y.; Shi, J.; Qu, Y.; Li, L.; Zhao, T.; Niu, Z.; Yang, R.; Gong, P. Assessing the ecological vulnerability of protected areas by using Big Earth Data. *Int. J. Digit Earth.* **2021**, *14*, 1624–1637. [\[CrossRef\]](#)
62. Zhang, Q.; Xu, C.-Y.; Yang, T. Variability of water resource in the Yellow River basin of past 50 years, China. *Water Resour. Manag.* **2009**, *23*, 1157–1170. [\[CrossRef\]](#)
63. Wohlfart, C.; Mack, B.; Liu, G.; Kuenzer, C. Multi-faceted land cover and land use change analyses in the Yellow River Basin based on dense Landsat time series: Exemplary analysis in mining, agriculture, forest, and urban areas. *Appl. Geogr.* **2017**, *85*, 73–88. [\[CrossRef\]](#)
64. Chen, Y.P.; Fu, B.J.; Zhao, Y.; Wang, K.B.; Zhao, M.M.; Ma, J.F.; Wu, J.H.; Xu, C.; Liu, W.G.; Wang, H. Sustainable development in the Yellow River Basin: Issues and strategies. *J. Clean. Prod.* **2020**, *263*, 121223. [\[CrossRef\]](#)

65. Liu, B.; Pan, L.; Qi, Y.; Guan, X.; Li, J. Land use and land cover change in the Yellow River Basin from 1980 to 2015 and its impact on the ecosystem services. *Land* **2021**, *10*, 1080. [[CrossRef](#)]
66. Feng, S.Y.; Liu, X.; Zhao, W.W.; Yao, Y.; Zhou, A.; Liu, X.X.; Pereira, P. Key areas of ecological restoration in Inner Mongolia based on ecosystem vulnerability and ecosystem service. *Remote Sens.* **2022**, *14*, 2729. [[CrossRef](#)]
67. Hu, W.M.; Li, G.; Gao, Z.H.; Jia, G.Y.; Wang, Z.C.; Li, Y. Assessment of the impact of the Poplar Ecological Retreat Project on water conservation in the Dongting Lake wetland region using the InVEST model. *Sci. Total Environ.* **2020**, *733*, 139423. [[CrossRef](#)]
68. Nelson, E.; Mendoza, G.; Regetz, J.; Polasky, S.; Tallis, H.; Cameron, D.; Chan, K.M.; Daily, G.C.; Goldstein, J.; Kareiva, P.M.; et al. Modeling multiple ecosystem services, biodiversity conservation, commodity production, and tradeoffs at landscape scales. *Front. Ecol. Environ.* **2009**, *7*, 4–11. [[CrossRef](#)]
69. Goldstein, J.H.; Caldarone, G.; Duarte, T.K.; Ennaanay, D.; Hannahs, N.; Mendoza, G.; Polasky, S.; Wolny, S.; Daily, G.C. Integrating ecosystem-service tradeoffs into land-use decisions. *Proc. Natl. Acad. Sci. USA* **2012**, *109*, 7565–7570. [[CrossRef](#)]
70. Liu, Z.; Wang, J.; Wang, X.; Wang, Y. Understanding the impacts of ‘Grain-for-Green’ land management practice on land greening dynamics over the Loess Plateau of China. *LUP* **2020**, *99*, 105084.
71. Estel, S.; Kuemmerle, T.; Alcántara, C.; Levers, C.; Prishchepov, A.; Hostert, P. Mapping farmland abandonment and recultivation across Europe using MODIS NDVI time series. *Remote Sens. Environ.* **2015**, *163*, 312–325. [[CrossRef](#)]
72. Wang, X.; Sun, Z.; Feng, X.; Ma, J.H.; Jia, Z.X.; Wang, X.X.; Zhou, J.T.; Zhang, X.R.; Yao, W.J.; Tu, Y. Identification of priority protected areas in Yellow River Basin and detection of key factors for its optimal management based on multi-scenario trade-off of ecosystem services. *Ecol. Eng.* **2023**, *194*, 107037. [[CrossRef](#)]
73. Wang, S.; Zhang, X.; Wu, T.; Yang, Y. The evolution of landscape ecological security in Beijing under the influence of different policies in recent decades. *Sci. Total Environ.* **2019**, *646*, 49–57. [[CrossRef](#)]
74. Zhao, Y.Z.; Zou, X.Y.; Cheng, H.; Jia, H.K.; Wu, Y.Q.; Wang, G.Y.; Zhang, C.L.; Gao, S.Y. Assessing the ecological security of the Tibetan plateau: Methodology and a case study for Lhaze County. *J. Environ. Manag.* **2006**, *80*, 120–131. [[CrossRef](#)]
75. Saaty, T.L. How to make a decision: The analytic hierarchy process. *Interfaces* **1994**, *24*, 19–43. [[CrossRef](#)]
76. Yu, L.; Wu, X.; Zheng, X.; Zheng, T.; Xin, J.; Walther, M. An index system constructed for ecological stress assessment of the coastal zone: A case study of Shandong, China. *J. Environ. Manag.* **2019**, *232*, 499–504. [[CrossRef](#)] [[PubMed](#)]
77. Huang, J.; Yu, H.; Han, D.; Zhang, G.; Wei, Y.; Huang, J.; An, L.; Liu, X.; Ren, Y. Declines in global ecological security under climate change. *Ecol. Indic.* **2020**, *117*, 106651. [[CrossRef](#)]
78. Zhao, M.; He, Z.; Du, J.; Chen, L.; Lin, P.; Fang, S. Assessing the effects of ecological engineering on carbon storage by linking the CA-Markov and InVEST models. *Ecol. Indic.* **2019**, *98*, 29–38. [[CrossRef](#)]
79. Hamel, P.; Chaplin-Kramer, R.; Sim, S.; Mueller, C. A new approach to modeling the sediment retention service (InVEST 3.0): Case study of the Cape Fear catchment, North Carolina, USA. *Sci. Total Environ.* **2015**, *524*, 166–177. [[CrossRef](#)]
80. Zhang, M.; Bao, Y.; Xu, J.; Han, A.; Liu, X.; Zhang, J.; Tong, Z. Ecological security evaluation and ecological regulation approach of East-Liao River basin based on ecological function area. *Ecol. Indic.* **2021**, *132*, 108255. [[CrossRef](#)]
81. Liu, D.; Yin, Z. Spatial-temporal pattern evolution and mechanism model of tourism ecological security in China. *Ecol. Indic.* **2022**, *139*, 108933. [[CrossRef](#)]
82. Liu, Y.; Zhao, C.; Liu, X.; Chang, Y.; Wang, H.; Yang, J.; Yang, X.; Wei, Y. The multi-dimensional perspective of ecological security evaluation and drive mechanism for Baishuijiang National Nature Reserve, China. *Ecol. Indic.* **2021**, *132*, 108295. [[CrossRef](#)]
83. Zhang, R.; Wang, C.; Xiong, Y. Ecological security assessment of China based on the Pressure-State-Response framework. *Ecol. Indic.* **2023**, *154*, 110647. [[CrossRef](#)]
84. Huang, Q.; Peng, B.; Wei, G.; Wan, A. Dynamic assessment and early warning of ecological security: A case study of the Yangtze river urban agglomeration. *Nat. Hazards* **2021**, *107*, 2441–2461. [[CrossRef](#)]
85. Meng, Z.; Li, C.; Deng, Y. Ecological security early-warning and its ecological regulatory countermeasures in the Tuojiang River Basin. *J. Ecol. Rural Environ.* **2009**, *25*, 1–8.
86. Xiao, D.; Chen, W. On the basic concepts and contents of ecological security. *J. Appl. Ecol.* **2002**, *13*, 354–358.
87. Yu, Y.; Hua, T.; Chen, L.; Zhang, Z.Q.; Pereira, P. Divergent Changes in Vegetation Greenness, Productivity, and Rainfall Use Efficiency Are Characteristic of Ecological Restoration Towards High-Quality Development in the Yellow River Basin, China. *Engineering* **2023**, *30*. [[CrossRef](#)]
88. Jing, W.L.; Yao, L.; Zhao, X.D.; Zhang, P.Y.; Liu, Y.X.X.; Xia, X.L.; Song, J.; Yang, J.; Li, Y.; Zhou, C.H. Understanding terrestrial water storage declining trends in the Yellow River Basin. *Geophys. Res. Atmos.* **2019**, *124*, 12963–12984. [[CrossRef](#)]
89. Li, C.J.; Fu, B.J.; Wang, S.; Stringer, L.C.; Zhou, W.X.; Ren, Z.B.; Hu, M.Q.; Zhang, Y.J.; Eodríguez-Caballero, E.; Weber, B.; et al. Climate-driven ecological thresholds in China’s drylands modulated by grazing. *Nat. Sustain.* **2023**, *6*, 1363–1372. [[CrossRef](#)]

**Disclaimer/Publisher’s Note:** The statements, opinions and data contained in all publications are solely those of the individual author(s) and contributor(s) and not of MDPI and/or the editor(s). MDPI and/or the editor(s) disclaim responsibility for any injury to people or property resulting from any ideas, methods, instructions or products referred to in the content.